Phenomenology of the Growth of Single Walled Aluminosilicate and Aluminogermanate Nanotubes

Sanjoy Mukherjee, and Sankar Nair
School of Chemical & Biomolecular Engineering, Georgia Tech, Atlanta GA 30332-0100

I. Introduction

Nanotubular materials[1] are important building blocks of a future nanotechnology based on synthesis of functional nanoparticles and their assembly into nanoscale devices with novel applications in areas such as electronics, biotechnology, sensing, separations, energy storage/management and catalysis. The discovery of carbon nanotubes[2] has stimulated extensive research on the synthesis, properties and applications of nanotubes, with the majority of studies being focused on the novel properties of carbon nanotubes. However, several problems in carbon nanotube technology remain to be overcome, e.g. the development of a low-temperature synthetic process with high yield as well as precise control over the nanotube dimensions and chirality, limitations of chemical composition, and the production of 'three-dimensionally nanoscale' carbon nanotube objects (i.e., single-walled objects smaller than 10 nm in both length and cross-section). To achieve their full potential, nanotechnological applications will ultimately require precise control over nanotube dimensions and monodispersity at length scales below 100 nm.

Inorganic nanotubes[3], nanorods and nanowires are being increasingly investigated for nanotechnological applications owing, among several factors, to the vast range of potential physicochemical properties afforded by inorganic materials. Several of these structures are synthesized using carbon nanotubes as templates and thus possess the same potential difficulty of control over nanoparticle dimensions. Most of the inorganic nanotubes synthesized to date, apart from molybdenum disulfide (MoS_2), are polydisperse and/or multiwalled materials[3-6]. In addition, they have high aspect ratios and are several hundred nanometers to microns in length. An apparent exception is the synthetic version of the naturally occurring nanotube mineral imogolite[7]. The synthesis and properties of these materials have been investigated to a significant extent over the years[7-12]. Imogolite is a single-walled nanotube (Figure 1a and 1b) whose wall structure is identical to a layer of aluminum (III) hydroxide (gibbsite); with isolated silicate groups bound on the inner wall. The nanotube has a periodic wall structure composed of six-membered aluminum hydroxide rings, with a repeat unit of approximately 0.85 nm along the nanotube axis[7]. The empirical formula of imogolite is $(OH)_3Al_2O_3SiOH$. The presence of hydroxyl groups on walls and rims makes the nanotube hydrophilic. Naturally occurring imogolite has an external diameter of around 2.0 nm and an internal diameter of around 1.0 nm[9]. The structural model shown in Figure 1 was proposed[7-9] based on solid-state NMR, TEM and XRD studies that established its close relation to the layered structure of gibbsite as well as the coordination and environment of the Al and Si atoms. Synthetic imogolite was prepared[10] from a millimolar aluminosilicate precursor solution at a temperature of 95ºC. The typical solid-state structure consists of nanotube bundles or ropes several microns in length. An aluminogermanate analog has also been successfully prepared by substitution of silicon with germanium in the synthesis solution[13]. However, from the limited amount of characterization data available, the aluminogermanate (Al-Ge) analogs appear considerably shorter than the aluminosilicate (Al-Si) nanotubes and their diameters are about 50% larger.

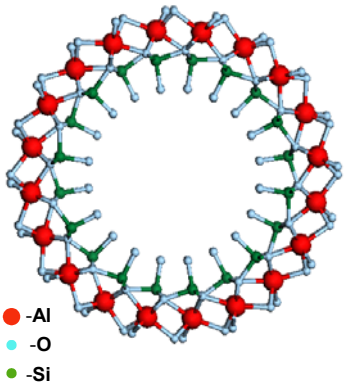

Figure I.1. Cross sectional view of the aluminosilicate nanotube imogolite.

From the perspective of nanomaterials engineering, we are particularly interested in the potential nanotechnological applications of inorganic nanotubes with well defined length and diameter, that can be synthesized via relatively mild chemistry, and which have technologically useful properties different from carbon nanotubes. Imogolite nanotubes have been investigated for use as a catalyst support[14, 15] and for methane storage [16]. However, we are investigating other potential applications for these nanotubes. For example, the Al-Ge nanotubes, which are as short as 10 nm and with an outside diameter of 3.3 nm (see Results and Discussion), are attractive candidates for use in artificial ion channel devices due to their well-defined solid-state structure, hydrophilic interior and short length. Artificial ion channels have high potential for biomolecule sensing devices, particularly for high speed DNA and protein analysis[17]. These devices operate by detecting chain biopolymers as they translocate through a nanoscale ion-conducting channel. The variation in the ion conductance of the channel, when correlated to the biopolymer properties, can lead to novel sensing strategies with single-molecule resolution and high speed. Intrinsic limitations on the stability and reliability of nanoscale ion channels made from 'soft matter' such as proteins, have led to a requirement for solid-state hydrophilic ion channels of appropriate length and diameter[18]. Similarly, others have proposed the construction of nanocomponents such as nanoelectrical cables (containing a conducting polymer wire with an insulating nanotube sheath) by threading of polymers into short nanotubes. A number of recent simulation studies[19-21] using carbon nanotube models (< 5 nm in length) have suggested the potential for the above applications. However, the synthesis of short, monodisperse nanotubes required for these applications is a difficult problem to tackle with current carbon nanotube technology.

Our investigations into the synthesis and properties of inorganic nanotubes indicate that imogolite Al-Si and Al-Ge nanotubes have unique properties (e.g., short length, hydrophilicity, ability to disperse in aqueous phase, well defined structure, and monodispersity) which make them attractive candidates for the above applications. Despite the potential nanotechnological applications of imogolite-like nanotubes, the phenomenology and mechanism of its formation are not well understood. Previous investigators have suggested a mechanism based on the formation of sheets/layers of gibbsite which eventually develop curvature due to the binding of silicate groups. The curvature results from the differing bond lengths of the Al-O and Si-O bonds (0.19 nm and 0.16 nm respectively), i.e., the tetravalent silicon atoms pull the oxygen atoms in the aluminum hydroxide layer into a curved cylinder. The formation of imogolite has been proposed to occur from the intermediate "proto-imogolite", which is presumably a sheet-like particle[11]. However, its structure could not be detected by TEM and its existence is

proposed based on the structure of imogolite. It was observed that the quantity of nanotubes seemed to grow substantially with the reaction time, with all the precursors being consumed by about 120 hours of synthesis time[22]. Thus it was suggested[22, 23] that the formation of "proto-imogolite" precursors took place early in the reaction, and these precursors provided nuclei to the growth and formation of nanotubes by polymerization. However, definitive experimental proof of this mechanism is lacking. In contrast to this kinetically driven mechanism, a thermodynamically driven self-assembly process could also operate. Figure 2 shows a schematic of the main events that are likely to occur in the each of the two possible mechanisms. In a kinetically driven growth, the nanotube length would increase substantially with synthesis time as growth units are added to the end of the nanotube; whereas in a thermodynamically controlled self assembly process, nanotubes of specific dimensions are expected to self-assemble as dictated by the precursor solution properties and the temperature. The two synthesis mechanisms hence require different approaches towards controlling the nanomaterial structure.

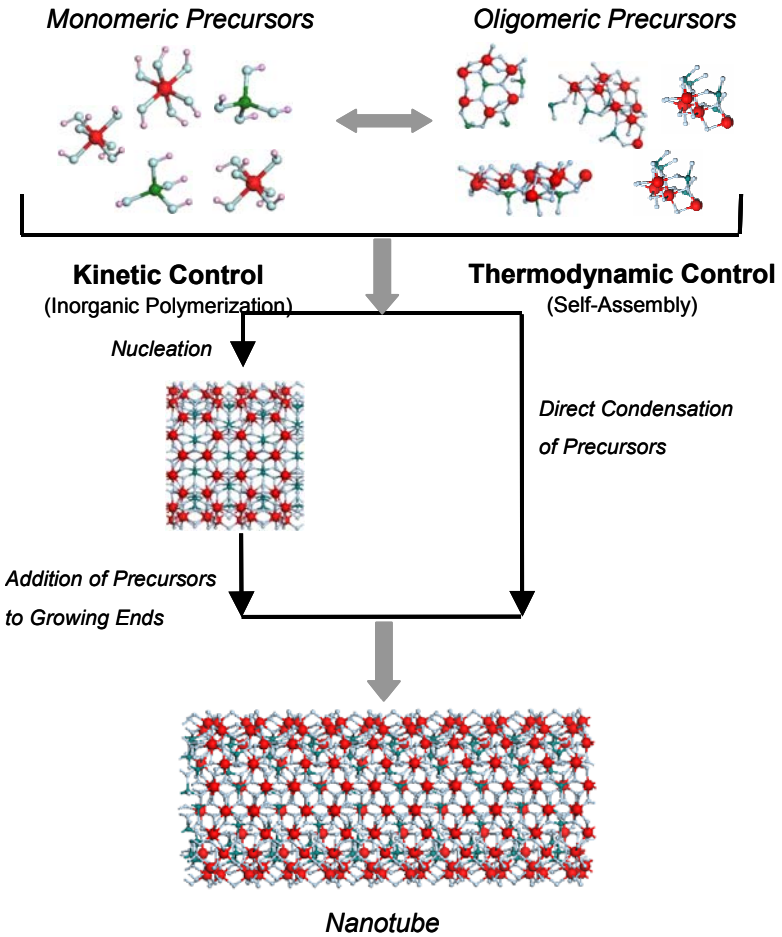

Figure I.2. Possible mechanisms of formation of nanotubes.

In the present paper, we report a systematic study of the growth of imogolite aluminosilicate and aluminogermanate nanotubes. Our approach is based on the use of a number of complementary characterization techniques to probe the dimensions, structure and morphology of the nanotubes both in solid state as well as aqueous phase, as a function of synthesis time. In particular, samples withdrawn at specific times (up to 120 hours) from the

nanotube synthesis reactor are then characterized using transmission electron microscopy (TEM), selected area electron diffraction (SAED), x-ray diffraction (XRD) and dynamic light scattering (DLS). TEM and XRD data were used to extract information on the morphology of the nanotubes and to propose a model for their packing in the solid state. SAED was used to ascertain the internal structure of the nanotubes as a function of growth time. Detailed mathematical analysis of DLS data provided quantitative information on the dimensions of the nanotubes in solution. The combination of characterization techniques revealed new aspects of the process of nanotube formation and structure, which are discussed below. The experimental evidence obtained in this paper is then discussed in the context of the two possible types of nanotube formation mechanisms. The phenomenology of aqueous phase Al-Si and Al-Ge nanotube growth as developed here is a required step towards understanding the mechanisms of formation of these nanoscale materials, and further using the insights gained to synthesize and apply new classes of functional nanomaterials.

II. Experimental Section

Tetraethylorthosilicate (TEOS) was added drop-wise to a stirred solution of 5 millimolar (mM) $AlCl_3$ solution until the Al:Si ratio was 1.8, and left to stand for 45 mins under vigorous stirring. Then a 0.1 N NaOH solution was added at the rate of 0.3 ml/min until the pH of the solution reached 5.0. The pH was brought down immediately to 4.5 by drop-wise addition of a solution containing 0.1 M HCl and 0.2 M of acetic acid. The resulting clear solution was allowed to stir for 3 hrs and then reacted at 95ºC under reflux conditions. A similar procedure was followed for the aluminogermanate nanotube except that TEOS was substituted by $GeCl_4$. For DLS analysis, 5 ml of the sample was filtered through a 0.2 μm pore size syringe filter to produce a dust-free sample containing only nanoscale particles. A drop of the sample was deposited on a formvar-backed copper TEM grid for electron microscopy and diffraction analysis. The remaining sample was transferred into a vessel under vigorous stirring. 0.1 N Ammonia solution was added carefully until the pH reached 8.0. At this point the solution turned murky and was centrifuged at 3000 rpm for 20 min. The supernatant was discarded and the gel acidified with a few drops of 12 N HCl. The resulting solution was immediately dialyzed against deionized water for 96 hrs to remove any unreacted precursors as well as sodium and chlorine ions. 5 ml of dialyzed solution was evaporated over a glass slide to deposit a film of nanotubes amenable to XRD and XPS (X-ray Photoelectron Spectroscopy) analysis. A portion of the dialyzed sample was freeze-dried and used for nitrogen adsorption measurements.

III. Results and Discussion

III.1 Solid-State Structure of Nanotubes: XRD, TEM and ED Characterization

Figures III.1a and III.2a shows TEM micrographs of the Al-Si and Al-Ge nanotubes at a synthesis time of 120 hours. The morphology of the Al-Si samples is that bundles of close-packed nanotubes, the lengths of the bundles being close to a micron. The bundles form a random fibrous network. On the other hand, the Al-Ge nanotubes are much shorter, do not form any fibrous mesostructures, and display a morphology consisting of nanotubes mostly standing upright on the surface of the polymeric TEM sample film. This distinct feature arising from the short length of the Al-Ge nanotubes enabled us to obtain clear TEM images down the axis of the Al-Ge nanotubes (Figure III.2a). The diameters of the Al-Si and Al-Ge nanotubes appear to be highly monodisperse, being measured as 2.2 nm and 3.3 nm (outer diameter)

respectively. In previous experimental and simulation studies, the packing of the nanotubes was assumed as hexagonal [24]. However, the appearance of XRD peaks at *d*-spacings of 1.611 nm (Al-Si, Figure III.1b) and 2.467 nm (Al-Ge, Figure III.2b) cannot be explained by a hexagonal packing model. After considering all the possible unit cell types, it was found that only monoclinic unit cells could index the XRD patterns. Remarkably, the monoclinic angle was found to be exactly the same (78º) for both the Al-Si and the Al-Ge nanotubes.

The SAED pattern shown in Figure III.3, mainly probe the structure within the individual nanotubes, and are important for tracking the formation of the nanotubes. With the crystallographic *c*-axis along the nanotube axis, the (006) and (004) reflections occurring at *d*-spacing of 0.14 nm and 0.21 nm are sharp and intense [8,7, 9, 12, 13, 25, 26], and arise from the periodic unit cell of approximately 0.85 nm in the *c*-direction. The (006) and (004) rings are thus taken as characteristic signatures that differentiate the nanotubes from any amorphous materials or other crystalline structures existing in the samples at various times during the reaction.

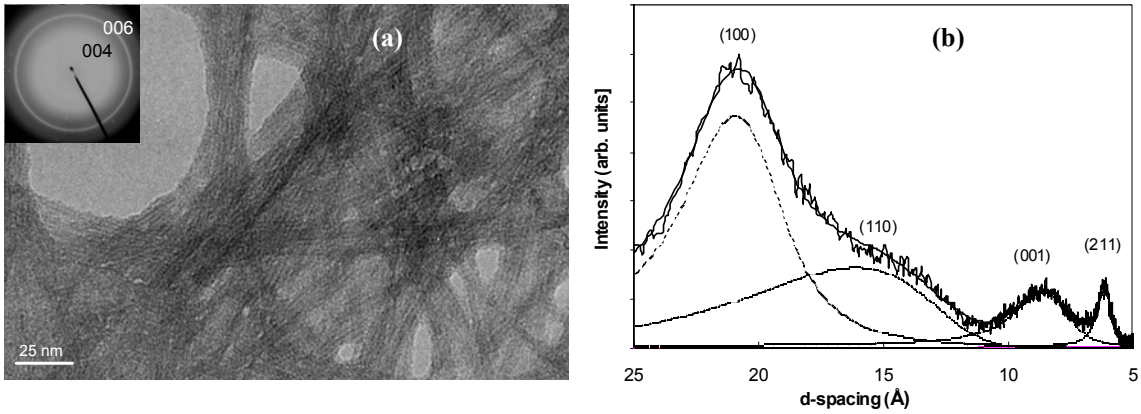

Figure III.1 (a) Transmission Electron Micrographs; and (b) XRD patterns of Al-Si NTs at synthesis time of 120 hours. The insets are SAED patterns obtained from the corresponding images.

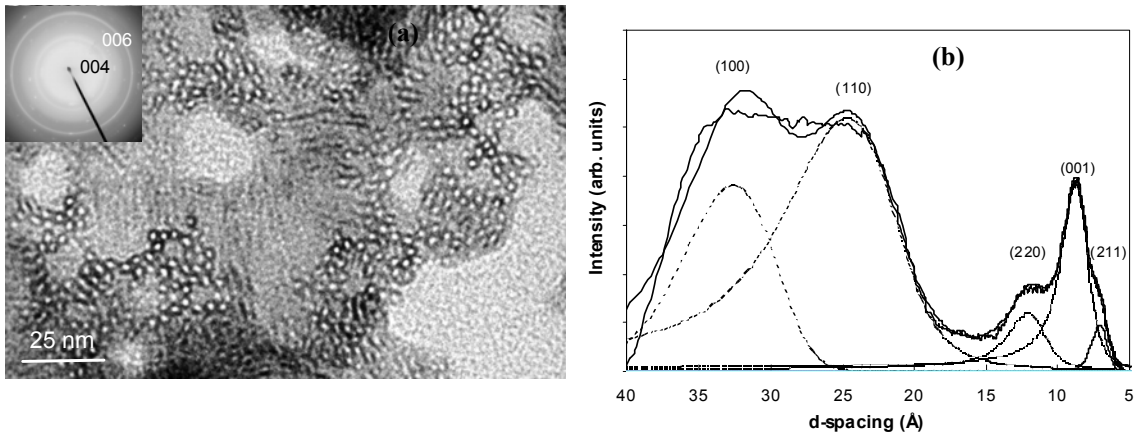

Figure III.2 (a) Transmission Electron Micrographs and (b) XRD patterns of Al-Ge NTs at synthesis time of 120 hours. The insets are SAED patterns obtained from the corresponding images.

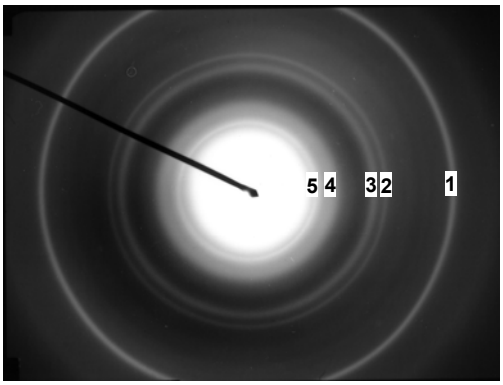

Reflections	d-spacing (nm)	hkl
1	0.14	006
2	0.21	004
3	0.22	063
4	0.32	071
5	0.43	002

Figure III.3 Selected Area Electron Diffraction Pattern of the Al-Si NTs. The numbers on the rings correspond to those tabulated in the Table. The diffraction rings are due to the atomic periodicity within a single nanotube.

III.2 Phenomenology of Growth of Nanotubes as a Function of Synthesis Time

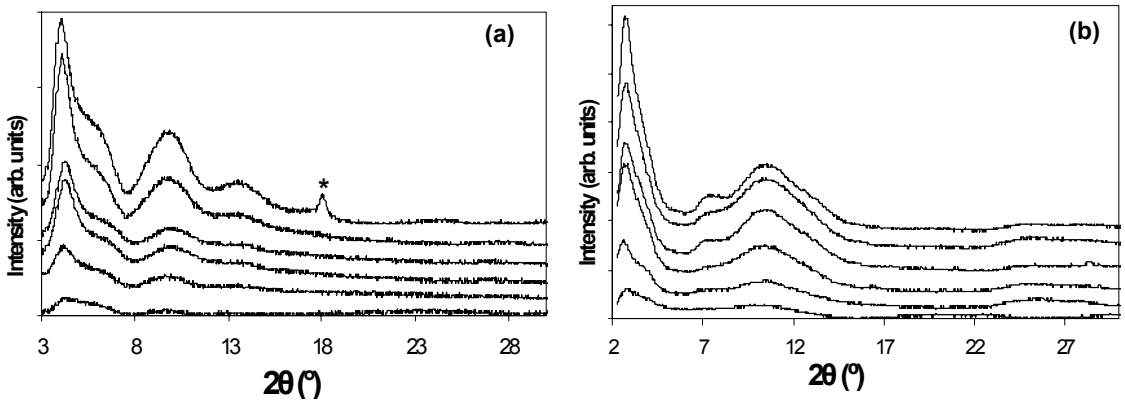

Figure III.4 X-ray diffraction spectra of (a) Al-Si NTs and (b) Al-Ge NTs at synthesis time of 10 hrs, 24 hrs, 48 hrs, 72 hrs, 96 hrs and 120 hrs respectively, arranged from bottom to top with increasing synthesis time.

Figures III.4a and III.4b shows the XRD patterns of Al-Si and Al-Ge nanotubes extracted from the reactor samples at reaction times of 10, 24, 48, 72 96 and 120 hrs. It is apparent that all the peaks seen in the 120-hr samples are clearly visible even at small reaction times (10 hrs). All the peaks increase in intensity as the reaction time is increased, showing clearly that the nanotubes are increasing in quantity, and indeed prefer the same solid-state packing arrangement throughout. Since the volume of sample dried on the glass slide was the same in all cases, the concentration of the nanotubes must be increasing with reaction time. The sharp peak appearing in the 120 hrs Al-Si sample (Figure III.4a) is believed to originate from a dense impurity phase that occasionally forms in the synthesis product.

A series of TEM micrographs in Figures III.5a-III.5c, shows the samples prepared directly from the Al-Si nanotube synthesis reactor at reaction times of 10, 72 and 120 hrs respectively. The SAED patterns are also inset in the Figures. It is clear that nanotubes form as early as 10 hrs. This is inferred from the morphology of the TEM images, and is well supported by the occurrence of the (006) and (004) reflections in all the SAED patterns.

Figures III.6a-III.6c shows the TEM micrographs of Al-Ge nanotubes at intermediate growth times of 10, 72, and 120 hrs; and the insets show the SAED patterns. All the micrographs clearly show the presence of nanotubes from as early as 10 hrs, and the reduction of amorphous materials with the increase in synthesis time. In the Al-Ge case however, the nanotubes are relatively short (~10 nm) as indicated before. Qualitative comparison of the images does not indicate any appreciable changes in the nanotube length and diameter, or observable high polydispersity in either the length or the diameter.

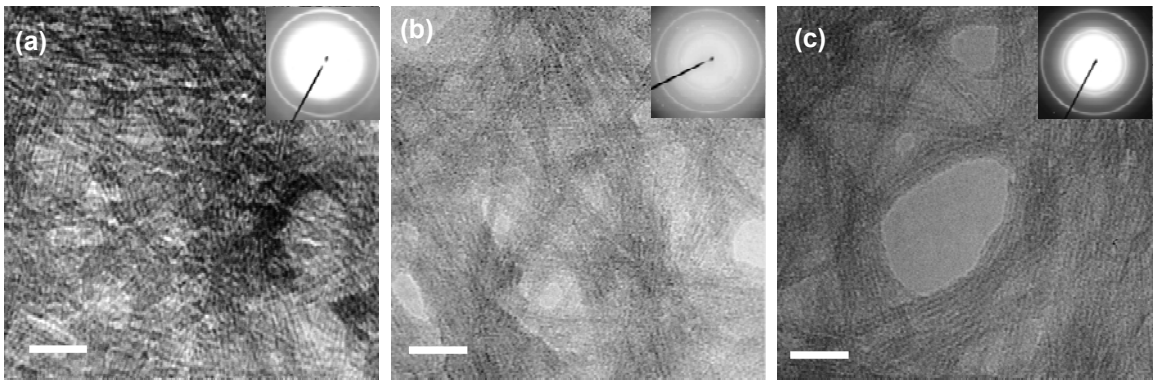

Figure III.5 Transmission electron micrographs of Al-Si NTs as a function of synthesis time of (a) 10 hrs (b) 72 hrs (c) 120 hrs. The insets show the corresponding SAED patterns. The scale bar is 25 nm.

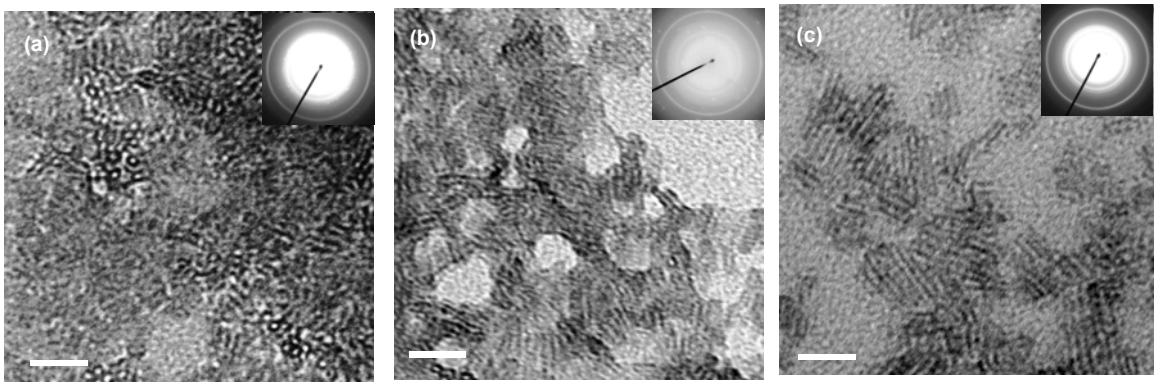

Figure III.6 Transmission electron micrographs of Al-Ge NTs as a function of synthesis time of (a) 10 hrs (b) 72 hrs (c) 120 hrs. The insets show the corresponding SAED patterns. The scale bar is 25 nm.

DLS is a useful technique for studying the dimensions of nanoparticles in solution at dilute concentrations. For a rigid rod nanoparticle undergoing Brownian translational and rotational motion in a solvent, the translational and rotational diffusivity coefficients D and Θ respectively are related as $L^2\Theta/D \sim 9$[27]. In particular, Θ has an L^{-3} dependence, where L is the length of the rod. When the rod length is short, the rotational diffusion becomes very rapid. If the time taken to rotationally circumscribe a sphere approaches the delay time ($\tau \sim 1\ \mu s$) of the autocorrelator, then the rapidly rotating rod can be approximated as a translationally diffusing sphere whose diameter equals the length of the rod. In our experiments the measured diffusion coefficients for the Al-Ge nanotubes were of the order of 5×10^{-7} cm^2/s, and the nanotube length as obtained from TEM micrographs was ~10 nm. Then $\Theta = 4.5 \times 10^6$ rad^2/s.

The time taken to circumscribe a sphere is given as: $\frac{2\pi^2}{\Theta}$ = 4.4 μs, which is close to the delay time of the autocorrelator. Thus, to the autocorrelator the rapidly rotating short rod is indistinguishable from a spherical nanoparticle whose diameter equals the length of the rod. Therefore, in the case of the short Al-Ge nanotubes, the length can be obtained in a simple manner from the diffusivity *D* via the Stokes-Einstein equation: $\frac{3\pi\eta_0 L}{kT} = D$. With an increase in the length of the rods (Al-Si nanotubes) the rotational motion becomes more sluggish and a full model for rigid rod diffusion (described below) can be used for data analysis.

The Siegert equatio [28] relates the normalized intensity autocorrelation function $g_2(t)$ with field autocorrelation function $g_1(t)$ as $g_2(t) = 1 + \beta|g_1(t)|^2$. Here β, the coherence factor [28], is an adjustable parameter (taken as unity in dilute aqueous suspensions). The full model for the field autocorrelation function of a suspension of nanorods of uniform diameter but polydisperse length is [29-31]:

$$g_1(t) = \int_0^\infty \left[a_0 \exp(-Q^2 Dt + Q^4 D^2 t/120\Theta) + a_2 \exp(-Q^2 Dt - 6\Theta t - Q^2 Dt/7)\right] P(L)\,dL \qquad (4)$$

Here *Q* is the momentum transfer given by *Q* = (4□*n*/□sin(□/2), where *n* is the refractive index of water, □ is the wavelength of the incident light, and □ is the scattering angle (90° in the present study). The function *P(L)* is the distribution function of the rod lengths. The prefactors a_0 and a_2 are given as:

$$a_0 = 1 - Q^2L^2/36 + 13Q^4L^4/32400 + Q^4L^2D/1080\Theta - Q^4D^2/720\Theta^2$$
$$a_2 = Q^4L^4/6480 - Q^4L^2D/1080\Theta + Q^4D^2/720\Theta^2 \qquad (5)$$

This model can be used to obtain the nanotube length from DLS data, employing the expression for the translational diffusivity *D* of a slightly bending nanorod [29-31]:

$$\frac{3\pi\eta_0 LD}{kT} = ln\left(\frac{L}{d}\right) + 0.3863 + 0.67(\chi L) + 0.01883(\chi L)^2 + O(\chi L)^3 \qquad (6)$$

Here η_0 is the viscosity of the aqueous solvent (0.89 cP at 25°C), χ is the inverse Kuhn length [32] which parameterizes the bending of the rods and which converges to zero for a perfectly rigid rod, *L* is the length of the rod and *d* is the outer diameter. The observed signal intensity was in the region of 10,000-250,000 counts per second in all cases. The autocorrelator produces $g_2(t)$ with a high signal-to-noise ratio by means of repeated scans on the sample (see Experimental Section). Then $g_1(t)$ was obtained from $g_2(t)$ according to the Siegert relation, and the diffusion model (Equations 4-6) was directly fitted to $g_1(t)$ via a nonlinear least squares algorithm developed in-house. Initially, a monodisperse suspension was assumed. The only fit parameters are the nanotube length (*L*) and the inverse Kuhn length (□). The diameter of the Al-Si nanotubes was taken as *d* = 2.2 nm based on the TEM images. The values of the

nanotube length were used in a subsequent fit incorporating a length distribution function *P(L)* of Gaussian form, i.e. $P(L) = \left(1/\sqrt{2\pi}\sigma_L\right).exp\left[-(L-\bar{L})^2/2\sigma_L^2\right]$.

The fitted lengths of the nanotubes from DLS data, as functions of synthesis time are shown in Figure V.7, for both Al-Si and Al-Ge nanotubes. The error bars on the fitted lengths are obtained by averaging the results from 4 independent samples taken in different experiments. An important result of this analysis is that the nanotubes do not grow in length substantially as a function of synthesis time. The Al-Si NTs are about 100 nm in length, whereas the Al-Ge nanotubes are about 10-15 nm in length. These results are well consistent with the detailed TEM observations.

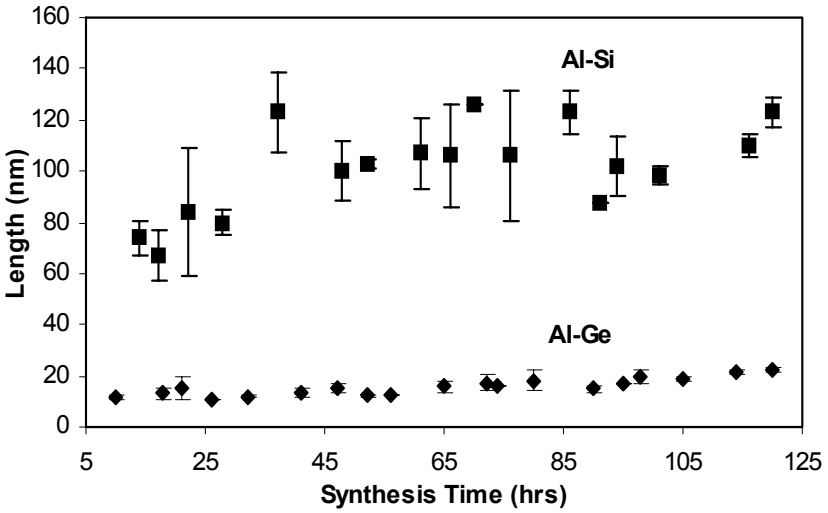

Figure III.7 The fitted lengths of the Al-Si NTs and Al-Ge NTs obtained from DLS experiments, as a function of synthesis time.

Conclusions

In the light of the present work, it is suggested that the nanotubes are the product of a thermodynamically controlled molecular self-assembly process. In other words, the formation of a small (10-100 nm) nanotubular molecule is the final step or the termination of the reaction, rather than a nucleation step for the growth of longer nanotubes. In this case, control over the nanotube dimensions is unlikely to be obtained by increasing the synthesis time or adding reactants continuously to the synthesis reactor in the hope of extending the nanotube length, but rather by thermodynamic control over the reaction chemistry. For example, the substitution of silicon with germanium leads to a substantial, yet precise, change in the nanotube diameter and length. Other possible methods of thermodynamic control include the use of organosilane precursors (which contain a Si-C bond). These could potentially lead to the formation of well-defined nanotubes with organic-functionalized interiors. From the viewpoint of technological applications, the prevalence of thermodynamic control has advantages in terms of the ability to obtain nanotubes whose dimensions are governed more precisely by the thermodynamics of the self assembly process. The 10 nm and 100 nm nanotubes can be regarded as nanocomponents that should be well amenable to applications in areas as diverse as nanocomposites and nanobiotechnology. The above synthetic and mechanistic issues, as well as applications of the Al-Si and Al-Ge nanotubes, are under detailed investigation in our laboratory.

VI. References

1. Lieber, C. M., One-dimensional nanostructures: Chemistry, physics & applications. *Solid State Communications* **1998,** 107, (11), 607-616.
2. Iijima, S., Helical Microtubules of Graphitic Carbon. *Nature* **1991,** 354, (6348), 56-58.
3. Rao, C. N. R.; Nath, M., Inorganic nanotubes. *Dalton Transactions* **2003**, (1), 1-24.
4. Patzke, G. R.; Krumeich, F.; Nesper, R., Oxidic nanotubes and nanorods - Anisotropic modules for a future nanotechnology. *Angewandte Chemie-International Edition* **2002,** 41, (14), 2446-2461.
5. Zhu, Y. Q.; Hsu, W. K.; Terrones, H.; Grobert, N.; Chang, B. H.; Terrones, M.; Wei, B. Q.; Kroto, H. W.; Walton, D. R. M.; Boothroyd, C. B.; Kinloch, I.; Chen, G. Z.; Windle, A. H.; Fray, D. J., Morphology, structure and growth of WS2 nanotubes. *Journal of Materials Chemistry* **2000,** 10, (11), 2570-2577.
6. Rosentsveig, R.; Margolin, A.; Feldman, Y.; Popovitz-Biro, R.; Tenne, R., WS2 nanotube bundles and foils. *Chemistry of Materials* **2002,** 14, (2), 471-473.
7. Cradwick, P. D.; Wada, K.; Russell, J. D.; Yoshinag.N; Masson, C. R.; Farmer, V. C., Imogolite, a Hydrated Aluminum Silicate of Tubular Structure. *Nature-Physical Science* **1972,** 240, (104), 187-&.
8. Russel, J. D.; McHardy, W. J.; Fraser, A. R., imogolote: A unique Aluminosilicate. *Clay Minerals* **1969,** 8, 87-99.
9. Wada, K.; Yoshinag.N, Structure of Imogolite. *American Mineralogist* **1969,** 54, (1-2), 50-&.
10. Farmer, V. C.; Fraser, A. R.; Tait, J. M., Synthesis of Imogolite - Tubular Aluminum Silicate Polymer. *Journal of the Chemical Society-Chemical Communications* **1977**, (13), 462-463.
11. Farmer, V. C.; Smith, B. F. L.; Tait, J. M., Stability, Free-Energy and Heat of Formation of Imogolite. *Clay Minerals* **1979,** 14, (2), 103-107.
12. Wada, S. I.; Eto, A.; Wada, K., Synthetic Allophane and Imogolite. *Journal of Soil Science* **1979,** 30, (2), 347-&.
13. Wada, S.; Wada, K., Effects of Substitution of Germanium for Silicon in Imogolite. *Clays and Clay Minerals* **1982,** 30, (2), 123-128.
14. Imamura, S.; Kokubu, T.; Yamashita, T.; Okamoto, Y.; Kajiwara, K.; Kanai, H., Shape-selective copper-loaded Imogolite catalyst. *Journal of Catalysis* **1996,** 160, (1), 137-139.
15. Marzan, L. L.; Philipse, A. P., Synthesis of Platinum Nanoparticles in Aqueous Host Dispersions of Inorganic (Imogolite) Rods. *Colloids and Surfaces a-Physicochemical and Engineering Aspects* **1994,** 90, (1), 95-109.
16. Ohashi, F.; Tomura, S.; Akaku, K.; Hayashi, S.; Wada, S. I., Characterization of synthetic imogolite nanotubes as gas storage. *Journal of Materials Science* **2004,** 39, (5), 1799-1801.
17. Nakane, J. J.; Akeson, M.; Marziali, A., Nanopore sensors for nucleic acid analysis. *Journal of Physics-Condensed Matter* **2003,** 15, (32), R1365-R1393.
18. Kong, C. Y.; Muthukumar, M., Modeling of polynucleotide translocation through protein pores and nanotubes. *Electrophoresis* **2002,** 23, (16), 2697-2703.
19. Gao, H. J.; Kong, Y.; Cui, D. X.; Ozkan, C. S., Spontaneous insertion of DNA oligonucleotides into carbon nanotubes. *Nano Letters* **2003,** 3, (4), 471-473.
20. Kalra, A.; Garde, S.; Hummer, G., Osmotic water transport through carbon nanotube membranes. *Proceedings of the National Academy of Sciences of the United States of America* **2003,** 100, (18), 10175-10180.
21. Hummer, G.; Rasaiah, J. C.; Noworyta, J. P., Water conduction through the hydrophobic channel of a carbon nanotube. *Nature* **2001,** 414, (6860), 188-190.
22. Wilson, M. A.; Lee, G. S. H.; Taylor, R. C., Tetrahedral rehydration during imogolite formation. *Journal of Non-Crystalline Solids* **2001,** 296, (3), 172-181.
23. Bursill, L. A.; Peng, J. L.; Bourgeois, L. N., Imogolite: an aluminosilicate nanotube material. *Philosophical Magazine a-Physics of Condensed Matter Structure Defects and Mechanical Properties* **2000,** 80, (1), 105-117.
24. Tamura, K.; Kawamura, K., Molecular dynamics modeling of tubular aluminum silicate: Imogolite. *Journal of Physical Chemistry B* **2002,** 106, (2), 271-278.
25. Barrett, S. M.; Budd, P. M.; Price, C., The Synthesis and Characterization of Imogolite. *European Polymer Journal* **1991,** 27, (7), 609-612.
26. Farmer, V. C.; Adams, M. J.; Fraser, A. R.; Palmieri, F., Synthetic Imogolite - Properties, Synthesis, and Possible Applications. *Clay Minerals* **1983,** 18, (4), 459-472.
27. Phalakornkul, J. K.; Gast, A. P.; Pecora, R., Rotational dynamics of rodlike polymers in a rod/sphere mixture. *Journal of Chemical Physics* **2000,** 112, (14), 6487-6494.

28. Claire, K.; Pecora, R., Translational and rotational dynamics of collagen in dilute solution. *Journal of Physical Chemistry B* **1997,** 101, (5), 746-753.
29. Yamakawa, H.; Fujii, M., Translational Friction Coefficient of Wormlike Chains. *Macromolecules* **1973,** 6, (3), 407-415.
30. Donkai, N.; Inagaki, H.; Kajiwara, K.; Urakawa, H.; Schmidt, M., Dilute-Solution Properties of Imogolite. *Makromolekulare Chemie-Macromolecular Chemistry and Physics* **1985,** 186, (12), 2623-2638.
31. Phalakornkul, J. K.; Gast, A. P.; Pecora, R., Rotational and translational dynamics of rodlike polymers: A combined transient electric birefringence and dynamic light scattering study. *Macromolecules* **1999,** 32, (9), 3122-3135.
32. Yilgor, I.; Yurtsever, E.; Erman, B., Conformational analysis of model poly(ether urethane) chains in the unperturbed state and under external forces. *Macromolecules* **2002,** 35, (26), 9825-9831.